THE JOURNAL OF PHYSICAL CHEMISTRY LETTERS
A JOURNAL OF THE AMERICAN CHEMICAL SOCIETY

pubs.acs.org/JPCL

Letter

Formally Exact Simulations of Mesoscale Exciton Diffusion in a Light-Harvesting 2 Antenna Nanoarray

Leonel Varvelo,[§] Jacob K. Lynd,[§] Brian Citty, Oliver Kühn, and Doran I. G. B. Raccah*

Cite This: *J. Phys. Chem. Lett.* 2023, 14, 3077−3083

Read Online

ACCESS | Metrics & More | Article Recommendations | Supporting Information

ABSTRACT: The photosynthetic apparatus of plants and bacteria combine atomically precise pigment−protein complexes with dynamic membrane architectures to control energy transfer on the 10−100 nm length scales. Recently, synthetic materials have integrated photosynthetic antenna proteins to enhance exciton transport, though the influence of artificial packing on the excited-state dynamics in these biohybrid materials is not fully understood. Here, we use the adaptive hierarchy of pure states (adHOPS) to perform a formally exact simulation of excitation energy transfer within artificial aggregates of light-harvesting complex 2 (LH2) with a range of packing densities. We find that LH2 aggregates support a remarkable exciton diffusion length ranging from 100 nm at a biological packing density to 300 nm at the densest packing previously suggested in an artificial aggregate. The unprecedented scale of these formally exact calculations also underscores the efficiency with which adHOPS simulates excited-state processes in molecular materials.

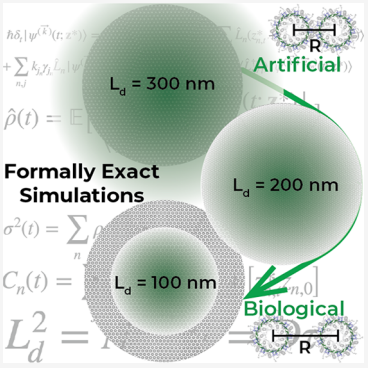

The ability to control energy transfer on the 10−100 nm length scale (often called the "mesoscale") is essential in designing new materials with applications in optoelectronics, photocatalysis, and light harvesting. The photosynthetic apparatus of plants and bacteria combine atomically precise structures of individual pigment−protein complexes with a dynamic membrane architecture that has both inspired new light-harvesting materials and stimulated advances in theoretical[1−6] and experimental[7−11] characterization of excitation energy transfer and charge separation. More recently, biohybrid materials that integrate photosynthetic proteins have demonstrated both convenient self-assembly and remarkable excitation energy transfer characteristics.[12−18]

Controlling excited-state processes in artificial assemblies of pigment−protein complexes requires understanding the mechanism of excitation transport on the mesoscale. Light-harvesting complex 2 (LH2) from purple bacteria is a widely studied biological antenna protein[19−22] that has been previously incorporated into artificial materials.[12,13] Early mechanistic studies of excitation energy transfer between LH2 pigment−protein complexes in biological assemblies suggest an incoherent mechanism of transport (i.e., excitations "hopping") between the dipole-allowed bright states.[21,23] Recent simulations of two-dimensional LH2 aggregates in artificial assemblies have suggested the possibility of coherent transport across multiple LH2 complexes on a relatively long 500 fs time scale (using the single-D1 Davydov ansatz)[20] or dark-state-mediated transport arising between close-packed LH2 pairs (using a Lindblad master equation).[19] On the other hand, a generalized master equation simulation suggests a dominantly incoherent mechanism of transport even for very close-packed LH2 rings.[24] While generalized master equations, such as generalized Förster theory, are accurate at biological inter-ring distances,[21] they assume weak electronic coupling between LH2 complexes. Because the densest proposed artificial aggregates of LH2 can have inter-ring electronic couplings that are an order of magnitude larger than those of their biological counterparts, assigning the corresponding mechanisms of transport remains a challenge.

A formally exact method for time-evolving exciton states provides a systematically improvable algorithm for calculating reduced density matrix dynamics to a desired precision with finite computational resources. While many formally exact methods for calculating exciton dynamics exist, such as the multi-D1 Davydov ansatz,[25] hierarchical equations of motion (HEOM),[26] hierarchy of pure states (HOPS),[27] time-evolving density operator with orthogonal polynomials (TEDOPA),[28] and quasi-adiabatic path integrals (QUAPI),[29] they are limited to small aggregates by the rapid scaling of their computational expense with the number of simulated molecules. Recent advances in reduced scaling techniques, such as modular path integrals,[30,31] tensor-contracted methods,[28,32−36] and adaptive basis set techniques,[37] raise the possibility of simulating excitation transport in mesoscale photosynthetic aggregates

Received: January 10, 2023
Accepted: March 6, 2023
Published: March 22, 2023

https://doi.org/10.1021/acs.jpclett.3c00086
J. Phys. Chem. Lett. 2023, 14, 3077−3083

using formally exact methods, but such calculations have not been reported to date.

In this paper, we perform the first formally exact simulations of mesoscale excitation transport in LH2 aggregates using the adaptive hierarchy of pure states (adHOPS).[37] Our calculations elucidate two sequential mechanisms of transport in artificial LH2 aggregates: a coherent mechanism that acts over a region 20 nm in diameter, followed by an incoherent mechanism that can support a remarkable excitation diffusion length of 300 nm.

We model excitation energy transport using an open quantum system Hamiltonian[38]

$$\hat{H} = \hat{H}_S + \sum_{n,q_n} \Lambda_{q_n} \hat{L}_n (\hat{a}_{q_n}^\dagger + \hat{a}_{q_n}) + \sum_{n,q_n} \hbar\omega_{q_n} (\hat{a}_{q_n}^\dagger \hat{a}_{q_n} + 1/2) \tag{1}$$

where $\hat{H}_S$ is the electronic (i.e., system) Hamiltonian, ω_{q_n} is the frequency of a harmonic oscillator with creation and annihilation operators $\hat{a}_{q_n}^\dagger$ and $\hat{a}_{q_n}$, respectively, and $\hat{L}_n$ is an operator ($\hat{L}_n = |n\rangle\langle n|$) that couples the nth pigment to its independent environment described by bath modes $\{q_n\}$ with coupling magnitudes Λ_{q_n}. The influence of the thermal environment on the electronic energy levels is described by a correlation function

$$C_n(t) = \frac{\hbar}{\pi} \int_0^\infty d\omega J_n(\omega)[\coth(\hbar\beta\omega/2)\cos(\omega t) - i\sin(\omega t)] \tag{2}$$

where $\beta = \frac{1}{k_B T}$ is the inverse temperature and $J_n(\omega)$ is the spectral density. Because complex exponentials form an overcomplete basis, we can decompose an arbitrary bath correlation function into a sum of exponentials called "correlation function modes", indexed by j_n,

$$C_n(t) = \sum_{j_n} g_{j_n} e^{-\gamma_{j_n} t/\hbar} \tag{3}$$

either numerically[39] or, in the case of several broad classes of spectral densities, analytically.[40,41]

We simulate the exciton dynamics using HOPS,[27] a formally exact solution to the open quantum system Hamiltonian (eq 1). In HOPS, the full state of the system and bath is expressed as a collection of wave functions indexed by a vector $\vec{k}$, where $|\psi_t^{(\vec{0})}\rangle$ is the physical wave function and the remainder are termed "auxiliary wave functions". The reduced density matrix for the system is given by an ensemble average ($\mathbb{E}[\cdot]$) over N_{traj} wave function trajectories

$$\rho_S = \mathbb{E}[|\psi^{(\vec{0})}(t; \mathbf{z}_t)\rangle\langle\psi^{(\vec{0})}(t; \mathbf{z}_t)|] \tag{4}$$

subject to a complex, stochastic noise $\mathbf{z}_t$ where components associated with individual thermal environments $z_{n,t}$ are defined by $\mathbb{E}[z_{n,t}] = 0$, $\mathbb{E}[z_{n,t}z_{n,s}] = 0$, and $\mathbb{E}[z_{n,t}^* z_{n,s}] = C_n(t-s)$. For the sake of notational simplicity, we will refer to $|\psi(t, \mathbf{z}_t)\rangle$ as $|\psi_t\rangle$. The time evolution of HOPS wave functions is then given by

$$\begin{aligned}\hbar\partial_t|\psi_t^{(\vec{k})}\rangle = &\left(-i\hat{H}_S - \vec{k}\cdot\vec{\gamma} - \Gamma_t + \sum_n \hat{L}_n(z_{n,t}^* + \xi_{n,t})\right)|\psi_t^{(\vec{k})}\rangle \\ &+ \sum_{n,j_n} k_{j_n}\gamma_{j_n}\hat{L}_n|\psi_t^{(\vec{k}-\vec{e}_{j_n})}\rangle \\ &- \sum_{n,j_n}\left(\frac{g_{j_n}}{\gamma_{j_n}}\right)(\hat{L}_n^\dagger - \langle\hat{L}_n^\dagger\rangle_t)|\psi_t^{(\vec{k}+\vec{e}_{j_n})}\rangle\end{aligned} \tag{5}$$

where

$$\xi_{n,t} = \frac{1}{\hbar}\int_0^t ds C_n^*(t-s)\langle L_n^\dagger\rangle_s \tag{6}$$

is a memory term that causes a drift in the effective noise

$$\langle\hat{L}_n^\dagger\rangle_t = \langle\psi_t^{(\vec{0})}|\hat{L}_n^\dagger|\psi_t^{(\vec{0})}\rangle \tag{7}$$

and

$$\begin{aligned}\Gamma_t = &\sum_n \langle\hat{L}_n\rangle_t \mathrm{Re}[z_{n,t}^* + \xi_{n,t}] - \sum_{n,j_n}\mathrm{Re}\left[\left(\frac{g_{j_n}}{\gamma_{j_n}}\right)\langle\psi_t^{(\vec{0})}|\hat{L}_n^\dagger|\psi_t^{(\vec{e}_{j_n})}\rangle\right] \\ &+ \sum_{n,j_n}\langle\hat{L}_n^\dagger\rangle_t \mathrm{Re}\left[\left(\frac{g_{j_n}}{\gamma_{j_n}}\right)\langle\psi_t^{(\vec{0})}|\psi_t^{(\vec{e}_{j_n})}\rangle\right]\end{aligned} \tag{8}$$

ensures normalization of the physical wave function. In these equations, k_{j_n} is the j_nth element of index vector $\vec{k}$ and $\vec{\gamma}$ is a vector of the exponential factors of the correlation function modes. Here we employ the "triangular truncation" scheme, which restricts the hierarchy of auxiliary wave functions to a finite depth k_{max}, such that $\left\{\vec{k}: \sum_i k_i \le k_{max}\right\}$, though other static filtering approaches have been proposed.[42]

The computational expense of HOPS scales poorly with system size due to a rapid increase in the number of auxiliary wave functions with the number of molecules. However, in an individual HOPS trajectory, coupling to the thermal environment induces a finite delocalization extent of the exciton in the basis of system states ($\mathbb{S}$).[37,43,44] The localization of a HOPS trajectory in the state basis engenders corresponding localization in the basis of auxiliary wave functions ($\mathbb{A}$).[37] The adHOPS algorithm leverages locality to reduce the computational expense for large molecular aggregates. At every update time (u_t), adHOPS constructs a reduced basis as a direct sum of reduced system and auxiliary bases ($\mathbb{S}_t \oplus \mathbb{A}_t$). It then truncates basis elements in order of increasing error until user-defined error bounds for the hierarchy (δ_A) and state (δ_S) bases are saturated. Previously, the adHOPS has demonstrated size-invariant [i.e., $O(1)$] scaling of the computational expense for a linear chain of molecules.[37]

We have implemented the adHOPS algorithm in MesoHOPS, an open-source Python package.[45] Additional details about both the algorithm and the calculation parameters are available in the Supporting Information. We check the convergence of adHOPS results by running a series of adHOPS ensembles with increasingly strict parameters until the characteristic observables are within 2% of the most exact calculations (section S4 of the Supporting Information).

The LH2 monomer (Figure 1a,b) contains two rings of bacteriochlorophyll (BChl) that absorb at 800 nm (B800 ring,

https://doi.org/10.1021/acs.jpclett.3c00086
J. Phys. Chem. Lett. 2023, 14, 3077−3083

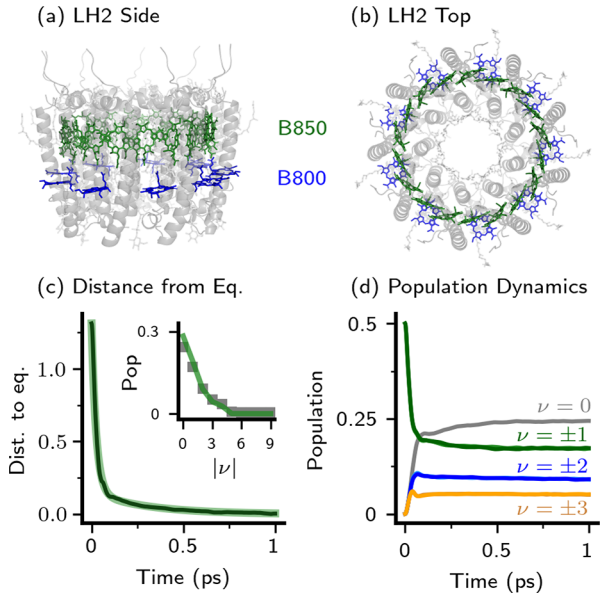

Figure 1. LH2 monomer. (a) Side view: the B850 ring (18 BChl molecules) and the B800 ring (9 BChl molecules) are colored green and blue, respectively. (b) Top view. (c) Distance from equilibrium as a function of time (black) compared to a biexponential fit (green). The inset shows the Boltzmann distribution (green line) compared to adHOPS equilibrium populations (gray squares) of eigenstates ordered by absolute index ($|\nu|$). (d) Population dynamics of the first seven eigenstates. σ = 160 cm^{-1} for site energy static disorder. Convergence parameters are listed in Table S6.

blue) and 850 nm (B850 ring, green). The B800 ring is comprised of 9 widely spaced and weakly coupled BChl molecules and funnels excitation to the B850 ring, which is responsible for transport between LH2 monomers. The tight packing of the 18 BChl molecules (organized into $\alpha\beta$ pairs) in the B850 ring gives rise to strong electronic couplings and delocalized eigenstates. Because inter-LH2 transport occurs predominately between B850 rings,[46] we neglect the B800 pigments found in Protein Data Bank entry 1NKZ.[47]

We model the Hamiltonian of the B850 ring using previously established parameters.[48] In the electronic ("system") Hamiltonian, the vertical excitation energies (or "site energies") of the α and β chlorophylls are 12690 and 12070 cm^{-1}, respectively, and the respective electronic couplings ($V_{n,m}$) within and between $\alpha\beta$ pairs are 307 and 237 cm^{-1} (section S1 of the Supporting Information). In keeping with previous spectroscopic assignments, we also include static disorder on the site energy of each chlorophyll as Gaussian fluctuations with a standard deviation σ of 160 cm^{-1} (section S5 of the Supporting Information).[22,48] Finally, following ref 48, we model the thermal environment of each pigment with a Drude–Lorentz spectral density characterized by a reorganization timescale (γ_{0_n} = 53 cm^{-1}) and reorganization energy (λ_n = 65 cm^{-1})

$$J_n(\omega) = 2\lambda_n\gamma_{0_n}\frac{\omega}{\omega^2 + \gamma_{0_n}^2}. \tag{9}$$

The corresponding correlation function is composed of one high-temperature mode, k_{Mats} Matsubara modes, and an additional mode to ensure $\mathrm{Im}[C_n(0)] = 0$ (section S2 of the Supporting Information). The ensemble is composed of an equal fraction of trajectories with excitations initiated in the ν = 1 or ν = −1 eigenstate of the donor B850.

Our model of the B850 ring captures the ultrafast relaxation of the bright-state excitation to an equilibrium distribution. We characterize the relaxation of the exciton population toward equilibrium in a monomer using the 1-norm of a difference vector $\|\underline{P}(t) - \underline{P}_{\mathrm{eq}}\|_1$, where $\underline{P}(t)$ and $\underline{P}_{\mathrm{eq}}$ are the eigenstate population vector of the B850 ring at time t and its equilibrium value, respectively. Using these parameters, the degenerate optically bright ($\nu = \pm 1$) states in the B850 ring relax to equilibrium on two time scales [τ_1 = 30 fs, and τ_2 = 300 fs (Figure 1c)]. The shortest and longest time scales of equilibration are associated with a rapid quasi-coherent transport across eigenstates and a slow relaxation of population into the ground state, respectively (Figure 1d). The time scales of relaxation calculated here are comparable to those found by global kinetic fits of B850 intraband relaxation in two-dimensional electronic spectroscopy (50 and 150 fs),[49] though care should be taken with the comparison of relaxation between spectroscopic and population-based observables. At long times, the equilibrium eigenstate populations (Figure 1c, inset) form a Boltzmann distribution, slightly perturbed by the electron-vibrational coupling.

We construct a hexagonally packed supercomplex containing 37 B850 rings (666 BChl) organized as three concentric shells around a donor ring (Figure 2a) with center-to-center ring distances (R) of 6.5 nm. This inter-ring distance represents the closest packing of LH2 proteins proposed for artificial aggregates.[19,50] The inter-ring couplings $\tilde{V}_{n,m}$ are calculated using the ideal dipole approximation

$$\tilde{V}_{n,m} = C\frac{\vec{d}_n\cdot\vec{d}_m - 3(\vec{d}_n\cdot\vec{r}_{n,m})(\vec{d}_m\cdot\vec{r}_{n,m})}{R_{n,m}^{\ 3}} \tag{10}$$

where the coupling constant C = 348 000 Å^3 cm^{-1}, $\vec{d}_n$ is a unit vector along the direction of the transition dipole moment of pigment n, and $\vec{r}_{n,m}$ ($R_{n,m}$) is the unit vector (distance) between Mg atoms in pigments n and m. In addition to the site energy static disorder included in each ring, we add an angular static disorder represented by randomly orienting the B850 rings in each trajectory. We find static disorder in the site energies suppresses transport while angular disorder has a negligible impact (sections S5 and S8 of the Supporting Information).

Exciton transport between LH2 in the 37-mer exhibits a change in dynamics between early (<100 fs) and late (>200 fs) time transport. Figure 2b plots the excitation population calculated with adHOPS summed across the sequential concentric shells of LH2 acceptors. Ultrafast exciton transport moves nearly 40% of excitations from the central donor LH2 (black line) to the first concentric shell of six acceptors (dark green line) within 100 fs. While the early time dynamics of the donor ring show a sinusoidal decay suggestive of a coherent mechanism, we observe slower subsequent transport into the second (medium green) and third (light green) acceptor shells. The change in exciton dynamics is mirrored in the mean-squared deviation (MSD) of the population distribution

$$\mathrm{MSD}(t) = \sum_n P_n(t)R_{0n}^{\ 2} \tag{11}$$

where P_n is the population of the nth B850 ring and n = 0 signifies the donor. Figure 2c shows that the MSD turns over from the early time superlinear behavior and reaches a linear form starting at 200 fs.

https://doi.org/10.1021/acs.jpclett.3c00086
J. Phys. Chem. Lett. 2023, 14, 3077−3083

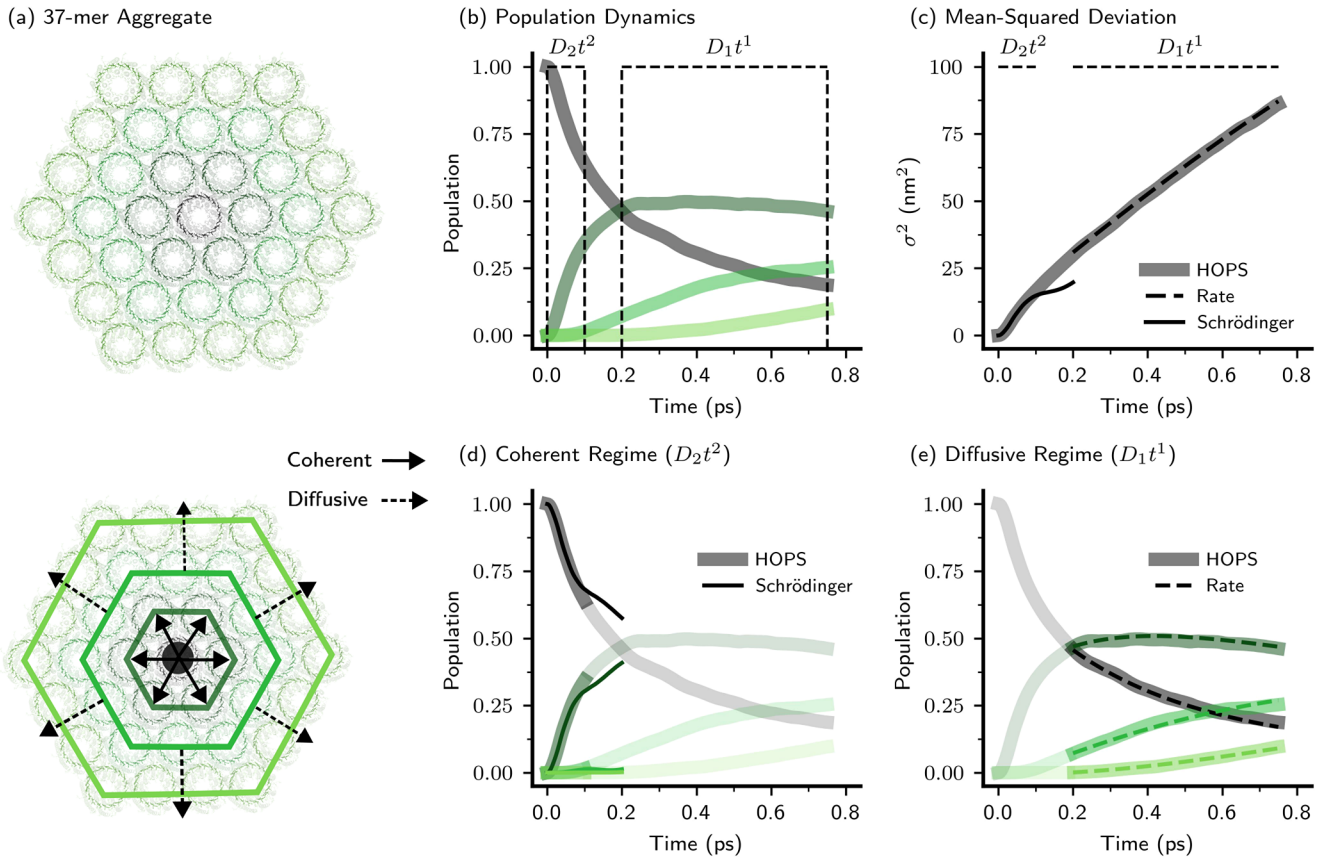

Figure 2. Exciton transport in a mesoscale aggregate of LH2. (a) LH2 37-mer (top) and schematic of a hexagonally packed B850 complex with three concentric shells (bottom). Solid arrows represent the length scale of coherent transport; dashed arrows represent the onset of diffusive transport. (b) adHOPS population dynamics of the donor and three concentric shells of B850 rings, color-coded to match the bottom part of panel a. (c) Mean-squared deviation (MSD) of the excitation. (d) Coherent early time exciton transport. (e) Diffusive late time exciton transport. σ = 160 cm^{-1} for site energy static disorder, and angular static disorder is given by randomly orienting all B850 rings in each trajectory. Convergence parameters are listed in Table S6.

On a sub-100 fs time scale, excitons move coherently across the donor and first concentric shell of the aggregate, covering an area of >100 nm^2. To assign the mechanism of transport, we compare our adHOPS dynamics with a matched calculation using a coherent equation of motion that excludes the vibrational environment (i.e., the Schrödinger equation) while including both site energy and angular static disorder. We find the purely coherent calculation (thin lines) reproduces the early time dynamics of both the MSD (Figure 2c) and concentric shell populations (Figure 2d). At longer time, however, the coherent calculation dramatically overestimates the population transport and the corresponding MSD (section S7 of the Supporting Information). The time scale on which vibrational fluctuations disrupt the coherent evolution of the electronic states is consistent with the reorganization time characterizing the spectral density ($\hbar/\gamma_{0_n} \approx 100$ fs).

On time scales longer than 200 fs, exciton transport occurs via an incoherent, diffusive mechanism. The linear character of the later time MSD curve suggests a diffusive transport mechanism in which time evolution of the vector of B850 ring populations ($\underline{P}(t)$) can be described by a kinetic model

$$\dot{\underline{P}}(t) = \underline{\underline{K}}\underline{P}(t) \tag{12}$$

with a rate matrix ($\underline{\underline{K}}$) that connects only nearest-neighbor rings via a symmetric transport rate κ. We find the average rate of transport calculated for an LH2 dimer (κ_{avg} = 0.53 ± 0.03 ps^{-1}) overestimates the long time rate because of the early time coherent dynamics. However, we can isolate an effective incoherent transport rate (κ_{dimer} = 0.44 ± 0.04 ps^{-1}) from the long time dynamics between the donor and acceptor LH2 (dashed line, Figure 3a), which can be characterized by a single exponential. Given the correct exciton population at 200 fs, this kinetic model (dashed lines) reproduces the long time dynamics of both the exciton MSD (Figure 2c) and concentric shell populations (Figure 2e).

Recently, a dark-state shelving mechanism has been proposed to modulate transport in close-packed LH2 aggregates,[19] but we find that inter-ring transport is dominated by coupling between bright states. Figure 3b compares the rates of population transport with an unaltered $\hat{H}_S$ (circles) and with inter-ring couplings via the dark states removed (squares) at various center-to-center dimer separations R. Neglecting dark-state-dependent inter-ring transport reduces the long time rate (κ_{dimer}) by 20−30% across the inter-ring separations (R) studied here. The limited role of dark states is consistent with inter-ring transport occurring on a time scale slower than that of intra-ring exciton relaxation, unlike the ultrafast transport between LH2 calculated with Linblad dynamics in ref 19. The incoherent (i.e., diffusive) transport between B850 rings controlled by bright states reflects the previously proposed supertransfer mechanism in which

https://doi.org/10.1021/acs.jpclett.3c00086
J. Phys. Chem. Lett. 2023, 14, 3077−3083

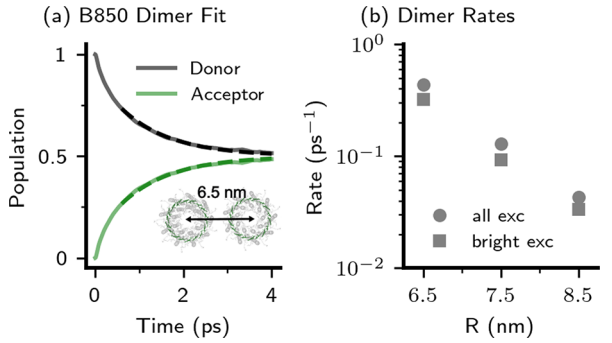

Figure 3. LH2 dimer rates. (a) Population transport calculated with adHOPS (solid lines) and a single-exponential fit starting at 600 fs (dashed lines) in an LH2 dimer with inter-ring separation R of 6.5 nm (inset). (b) Transport rates for an LH2 dimer with an inter-ring separation of R when all couplings are allowed (circles) and when inter-ring couplings involving dark states are neglected (squares). In all cases, σ = 160 cm^{-1} for site energy static disorder, and angular static disorder is given by randomly orienting both B850 rings in each trajectory. Convergence parameters are listed in Table S6.

delocalization around the B850 ring leads to enhanced exciton dipole moments and accelerated transport.[51−55]

At this point, the mesoscale nature of the 37-mer becomes clear: it is the smallest aggregate sufficient to observe the turnover from the short time coherent to long time diffusive transport mechanisms and cannot be fully described by approximate methods limited to either regime. The early time coherent mechanism can be characterized with a nearest-neighbor model composed of the donor ring and first concentric shell of acceptors. However, by the onset of diffusive transport (200 fs), the second concentric shell of B850 acceptor rings already contains nearly 10% of the exciton population. As a result, characterizing diffusive transport without edge effects requires a third concentric shell and an aggregate containing 37 LH2 complexes and a total of 666 bacteriochlorophylls.

For sufficiently large LH2 aggregates, our kinetic model predicts an excitation diffusion length (L_d) that greatly exceeds that of prototypical organic semiconductors, even for the relatively loose packing associated with biological membranes. Table 1 reports the excitation diffusion length in the kinetic

Table 1. LH2 Exciton Diffusion Lengths in a Hexagonally Packed Lattice

R (nm)	D_1[a] (nm^2/ps)	L_d[a] (nm)
6.5	110 ± 10	330 ± 20
7.5	43 ± 3	210 ± 6
8.5	19 ± 1	140 ± 4

[a]The uncertainty represents the 95% confidence interval.

model of an infinite aggregate (section S10 of the Supporting Information) determined by

$$L_d^2 = 6R^2\kappa_{dimer}\tau \equiv D\tau \quad (13)$$

where the factor of 6 arises from hexagonal packing, R is the packing distance, κ_{dimer} is the rate of transport between dimers, and τ is the lifetime of the exciton (assumed to be 1 ns).[56] At a biologically relevant inter-ring distance of 8.5 nm, our excitation diffusion length (L_d = 140 nm) is consistent with a previous order of magnitude estimate[57] and greatly exceeds those of boron subnaphthalocyanine chloride (21 nm), fullerene (19 nm), and other prototypical organic semiconductors (<30 nm).[58,59] Moreover, our rate of transport at R = 8.5 nm is smaller than some previous estimates (e.g., 0.241 ps^{-1} in ref 24), suggesting other LH2 Hamiltonians proposed in the literature could support even longer excitation diffusion lengths.

We conclude that LH2 aggregates support exciton transport on length scales exceeding those of similar artificial and natural materials. Excitons in tightly packed LH2 aggregates exhibit a brief coherent period (<100 fs) in which they rapidly migrate from the donor to the nearest-neighbor B850 rings, covering a region with a diameter of 20 nm. Following vibrational reorganization, diffusion continues via an incoherent "hopping" mechanism mediated by bright-state coupling. Excitonic hopping between B850 rings supports long-range diffusion even at biological packing distances (R = 8.5 nm, and L_d = 140 nm). Moreover, in artificially close-packed LH2 aggregates, our calculations suggest the exciton diffusion length can reach 300 nm, a full order of magnitude larger than a prototypical organic semiconductor, making LH2 a promising antenna system for biohybrid materials. Finally, we note that LH2 complexes, despite belonging to the evolutionarily "early" anoxygenic purple bacteria, support a surprisingly large L_d compared to that previously calculated for the oxygenic photosystem II membrane (L_d = 50 nm),[60,61] suggesting that the need for regulation rather than long-range excitation energy transport may have driven the design of antenna complexes in higher plants.

In this paper, we have reported a formally exact simulation of exciton dynamics in a mesoscale photosynthetic aggregate consisting of an unprecedented 37 LH2 complexes with a total of 666 bacteriochlorophylls. While some previous studies have simulated large LH2 aggregates using approximate methods, the current calculations provide an important benchmark result where the accuracy of the simulation is limited by only the parametrization of the model Hamiltonian. Our results also demonstrate that adHOPS is suitable for calculations of mesoscale molecular materials to address mechanistic questions about excited-state processes. We expect the continued development of adHOPS will enable a new generation of simulations capable of probing larger and more complex materials to reveal new strategies for controlling excited-state processes.

■ ASSOCIATED CONTENT

Data Availability Statement

Simplified generation scripts and packaged data for main text figures[62] and the specific version of MesoHOPS used for the calculations reported[63] are available on Zenodo.

Supporting Information

The Supporting Information is available free of charge at https://pubs.acs.org/doi/10.1021/acs.jpclett.3c00086.

Methodological details, all calculation parameters, convergence studies, further analysis of mechanisms of transport in terms of bright and dark states and coherent models, and comparison of different types of static disorder (PDF)

Transparent Peer Review report available (PDF)

https://doi.org/10.1021/acs.jpclett.3c00086
J. Phys. Chem. Lett. 2023, 14, 3077−3083

AUTHOR INFORMATION

Corresponding Author

Doran I. G. B. Raccah − *Department of Chemistry, Southern Methodist University, Dallas, Texas 75275, United States;* orcid.org/0000-0001-8322-7371; Email: doranb@smu.edu

Authors

Leonel Varvelo − *Department of Chemistry, Southern Methodist University, Dallas, Texas 75275, United States;* orcid.org/0000-0002-2013-1177

Jacob K. Lynd − *Department of Chemistry, Southern Methodist University, Dallas, Texas 75275, United States;* orcid.org/0000-0002-0762-8584

Brian Citty − *Department of Chemistry, Southern Methodist University, Dallas, Texas 75275, United States*

Oliver Kühn − *Institute of Physics, University of Rostock, 18059 Rostock, Germany;* orcid.org/0000-0002-5132-2961

Complete contact information is available at: https://pubs.acs.org/10.1021/acs.jpclett.3c00086

Author Contributions

[§]Co-first authors. These authors contributed equally, and authorship order was determined by a coin toss. All authors agree that these authors may list themselves in either order for their CV/resume and other purposes

Notes

The authors declare no competing financial interest.

ACKNOWLEDGMENTS

The authors thank Bailey Raber and Mohamed El Refaiy for assistance working with the protein structure and the electronic Hamiltonian for the extended aggregates, Julian Schmidt for helpful discussions and testing of a preliminary version of the adHOPS code, and Tarun Gera for editing and review. L.V., B.C., and D.I.G.B.R. acknowledge support from the Robert A. Welch Foundation (Grant N-2026-20200401). J.K.L. acknowledges support from a Moody Fellowship. O.K. acknowledges funding by the Deutsche Forschungsgemeinschaft - SFB 1477 "Light-Matter Interactions at Interfaces" (Project 441234705).

REFERENCES

(1) Sumi, H. Theory on Rates of Excitation-Energy Transfer Between Molecular Aggregates through Distributed Transition Dipoles with Application to the Antenna System in Bacterial Photosynthesis. *J. Phys. Chem. B* **1999**, *103*, 252−260.

(2) Scholes, G. D.; Jordanides, X. J.; Fleming, G. R. Adapting the Förster Theory of Energy Transfer for Modeling Dynamics in Aggregated Molecular Assemblies. *J. Phys. Chem. B* **2001**, *105*, 1640−1651.

(3) Jang, S.; Newton, M. D.; Silbey, R. J. Multichromophoric Förster Resonance Energy Transfer. *Phys. Rev. Lett.* **2004**, *92*, 218301.

(4) Yang, M.; Fleming, G. R. Influence of Phonons on Exciton Transfer Dynamics: Comparison of the Redfield, Forster, and Modified Redfield Equations. *Chem. Phys.* **2002**, *282*, 163−180.

(5) Ishizaki, A.; Fleming, G. R. Unified Treatment of Quantum Coherent and Incoherent Hopping Dynamics in Electronic Energy Transfer: Reduced Hierarchy Equation Approach. *J. Chem. Phys.* **2009**, *130*, 234111.

(6) Rebentrost, P.; Mohseni, M.; Kassal, I.; Lloyd, S.; Aspuru-Guzik, A. Environment-Assisted Quantum Transport. *New J. Phys.* **2009**, *11*, 033003.

(7) Brixner, T.; Stenger, J.; Vaswani, H. M.; Cho, M.; Blankenship, R. E.; Fleming, G. R. Two-Dimensional Spectroscopy of Electronic Couplings in Photosynthesis. *Nature* **2005**, *434*, 625−628.

(8) Harel, E.; Fidler, A. F.; Engel, G. S. Single-Shot Gradient-Assisted Photon Echo Electronic Spectroscopy. *J. Phys. Chem. A* **2011**, *115*, 3787−3796.

(9) Dahlberg, P. D.; Ting, P.-C.; Massey, S. C.; Allodi, M. A.; Martin, E. C.; Hunter, C. N.; Engel, G. S. Mapping the Ultrafast Flow of Harvested Solar Energy in Living Photosynthetic Cells. *Nat. Commun.* **2017**, *8*, 988.

(10) Arsenault, E. A.; Yoneda, Y.; Iwai, M.; Niyogi, K. K.; Fleming, G. R. Vibronic Mixing Enables Ultrafast Energy Flow in Light-Harvesting Complex II. *Nat. Commun.* **2020**, *11*, 1460.

(11) Biswas, S.; Kim, J.; Zhang, X.; Scholes, G. D. Coherent Two-Dimensional and Broadband Electronic Spectroscopies. *Chem. Rev.* **2022**, *122*, 4257−4321.

(12) Reynolds, N. P.; Janusz, S.; Escalante-Marun, M.; Timney, J.; Ducker, R. E.; Olsen, J. D.; Otto, C.; Subramaniam, V.; Leggett, G. J.; Hunter, C. N. Directed Formation of Micro- and Nanoscale Patterns of Functional Light-Harvesting LH2 Complexes. *J. Am. Chem. Soc.* **2007**, *129*, 14625−14631.

(13) Escalante, M.; Maury, P.; Bruinink, C. M.; van der Werf, K.; Olsen, J. D.; Timney, J. A.; Huskens, J.; Neil Hunter, C.; Subramaniam, V.; Otto, C. Directed Assembly of Functional Light Harvesting Antenna Complexes onto Chemically Patterned Surfaces. *Nanotechnology* **2008**, *19*, 025101.

(14) Escalante, M.; Zhao, Y.; Ludden, M. J. W.; Vermeij, R.; Olsen, J. D.; Berenschot, E.; Hunter, C. N.; Huskens, J.; Subramaniam, V.; Otto, C. Nanometer Arrays of Functional Light Harvesting Antenna Complexes by Nanoimprint Lithography and Host-Guest Interactions. *J. Am. Chem. Soc.* **2008**, *130*, 8892−8893.

(15) Vasilev, C.; Johnson, M. P.; Gonzales, E.; Wang, L.; Ruban, A. V.; Montano, G.; Cadby, A. J.; Hunter, C. N. Reversible Switching Between Nonquenched and Quenched States in Nanoscale Linear Arrays of Plant Light-Harvesting Antenna Complexes. *Langmuir* **2014**, *30*, 8481−8490.

(16) Mancini, J. A.; Kodali, G.; Jiang, J.; Reddy, K. R.; Lindsey, J. S.; Bryant, D. A.; Dutton, P. L.; Moser, C. C. Multi-Step Excitation Energy Transfer Engineered in Genetic Fusions of Natural and Synthetic Light-Harvesting Proteins. *J. R. Soc. Interface.* **2017**, *14*, 20160896.

(17) Yoneda, T.; Tanimoto, Y.; Takagi, D.; Morigaki, K. Photosynthetic Model Membranes of Natural Plant Thylakoid Embedded in a Patterned Polymeric Lipid Bilayer. *Langmuir* **2020**, *36*, 5863−5871.

(18) Kim, Y. J.; Hong, H.; Yun, J.; Kim, S. I.; Jung, H. Y.; Ryu, W. Photosynthetic Nanomaterial Hybrids for Bioelectricity and Renewable Energy Systems. *Adv. Mater.* **2021**, *33*, 2005919.

(19) Mattioni, A.; Caycedo-Soler, F.; Huelga, S. F.; Plenio, M. B. Design Principles for Long-Range Energy Transfer at Room Temperature. *Phys. Rev. X.* **2021**, *11*, 041003.

(20) Zheng, F.; Chen, L.; Gao, J.; Zhao, Y. Fully Quantum Modeling of Exciton Diffusion in Mesoscale Light Harvesting Systems. *Materials* **2021**, *14*, 3291.

(21) Strümpfer, J.; Schulten, K. Light Harvesting Complex II B850 Excitation Dynamics. *J. Chem. Phys.* **2009**, *131*, 225101.

(22) Scholes, G. D.; Fleming, G. R. On the Mechanism of Light Harvesting in Photosynthetic Purple Bacteria: B800 to B850 Energy Transfer. *J. Phys. Chem. B* **2000**, *104*, 1854−1868.

(23) Jimenez, R.; Dikshit, S. N.; Bradforth, S. E.; Fleming, G. R. Electronic Excitation Transfer in the LH2 Complex of Rhodobacter sphaeroides. *J. Phys. Chem.* **1996**, *100*, 6825−6834.

(24) Jang, S. J. Robust and Fragile Quantum Effects in the Transfer Kinetics of Delocalized Excitons between B850 Units of LH2 Complexes. *J. Phys. Chem. Lett.* **2018**, *9*, 6576−6583.

(25) Chen, L.; Borrelli, R.; Zhao, Y. Dynamics of Coupled Electron−Boson Systems with the Multiple Davydov D1 Ansatz and the Generalized Coherent State. *J. Phys. Chem. A* **2017**, *121*, 8757−8770.

(26) Tanimura, Y. Numerically "Exact" Approach to Open Quantum Dynamics: The Hierarchical Equations of Motion (HEOM). *J. Chem. Phys.* **2020**, *153*, 020901.
(27) Suess, D.; Eisfeld, A.; Strunz, W. T. Hierarchy of Stochastic Pure States for Open Quantum System Dynamics. *Phys. Rev. Lett.* **2014**, *113*, 150403.
(28) Tamascelli, D.; Smirne, A.; Lim, J.; Huelga, S. F.; Plenio, M. B. Efficient Simulation of Finite-Temperature Open Quantum Systems. *Phys. Rev. Lett.* **2019**, *123*, 090402.
(29) Makri, N. Improved Feynman Propagators on a Grid and Non-Adiabatic Corrections Within the Path Integral Framework. *Chem. Phys. Lett.* **1992**, *193*, 435.
(30) Makri, N. Communication: Modular Path Integral: Quantum Dynamics via Sequential Necklace Linking. *J. Chem. Phys.* **2018**, *148*, 101101.
(31) Makri, N. Modular Path Integral Methodology for Real-Time Quantum Dynamics. *J. Chem. Phys.* **2018**, *149*, 214108.
(32) Borrelli, R.; Dolgov, S. Expanding the Range of Hierarchical Equations of Motion by Tensor-Train Implementation. *J. Phys. Chem. B* **2021**, *125*, 5397−5407.
(33) Yan, Y.; Xu, M.; Li, T.; Shi, Q. Efficient Propagation of the Hierarchical Equations of Motion Using the Tucker and Hierarchical Tucker Tensors. *J. Chem. Phys.* **2021**, *154*, 194104.
(34) Gao, X.; Ren, J.; Eisfeld, A.; Shuai, Z. Non-Markovian Stochastic Schrödinger Equation: Matrix-Product-State Approach to the Hierarchy of Pure States. *Phys. Rev. A* **2022**, *105*, L030202.
(35) Somoza, A. D.; Marty, O.; Lim, J.; Huelga, S. F.; Plenio, M. B. Dissipation-Assisted Matrix Product Factorization. *Phys. Rev. Lett.* **2019**, *123*, 100502.
(36) Strathearn, A.; Kirton, P.; Kilda, D.; Keeling, J.; Lovett, B. W. Efficient Non-Markovian Quantum Dynamics Using Time-Evolving Matrix Product Operators. *Nat. Commun.* **2018**, *9*, 3322.
(37) Varvelo, L.; Lynd, J. K.; Bennett, D. I. G. Formally Exact Simulations of Mesoscale Exciton Dynamics in Molecular Materials. *Chem. Sci.* **2021**, *12*, 9704−9711.
(38) Schröter, M.; Ivanov, S. D.; Schulze, J.; Polyutov, S. P.; Yan, Y.; Pullerits, T.; Kühn, O. Exciton-Vibrational Coupling in the Dynamics and Spectroscopy of Frenkel Excitons in Molecular Aggregates. *Phys. Rep.* **2015**, *567*, 1−78.
(39) Hartmann, R.; Strunz, W. T. Exact Open Quantum System Dynamics Using the Hierarchy of Pure States (HOPS). *J. Chem. Theory Comput.* **2017**, *13*, 5834−5845.
(40) Ritschel, G.; Eisfeld, A. Analytic Representations of Bath Correlation Functions for Ohmic and Superohmic Spectral Densities Using Simple Poles. *J. Chem. Phys.* **2014**, *141*, 094101.
(41) Meier, C.; Tannor, D. J. Non-Markovian Evolution of the Density Operator in the Presence of Strong Laser Fields. *J. Chem. Phys.* **1999**, *111*, 3365−3376.
(42) Zhang, P.-P.; Bentley, C. D. B.; Eisfeld, A. Flexible Scheme to Truncate the Hierarchy of Pure States. *J. Chem. Phys.* **2018**, *148*, 134103.
(43) Schack, R.; Brun, T. A.; Percival, I. C. Quantum State Diffusion, Localization and Computation. *J. Phys. A* **1995**, *28*, 5401.
(44) Rigo, M.; Mota-Furtado, F.; O'Mahony, P. F. Continuous Stochastic Schrödinger Equations and Localization. *J. Phys. A* **1997**, *30*, 7557.
(45) Varvelo, L.; Lynd, J. K.; City, B.; Raccah, D. I. G. B. *MesoHOPS*, ver. 1.3.0; MesoscienceLab/mesohops, 2023; DOI: 10.5281/zenodo.7581955.
(46) Hu, X.; Ritz, T.; Damjanović, A.; Autenrieth, F.; Schulten, K. Photosynthetic Apparatus of Purple Bacteria. *Q. Rev. Biophys.* **2002**, *35*, 1−62.
(47) Papiz, M. Z.; Prince, S. M.; Howard, T.; Cogdell, R. J.; Isaacs, N. W. The Structure and Thermal Motion of the B800−850 LH2 Complex from Rps. Acidophila at 2.0Å Resolution and 100K: New Structural Features and Functionally Relevant Motions. *J. Mol. Biol.* **2003**, *326*, 1523−1538.
(48) Smyth, C.; Oblinsky, D. G.; Scholes, G. D. B800−B850 Coherence Correlates with Energy Transfer Rates in the LH2 Complex of Photosynthetic Purple Bacteria. *Phys. Chem. Chem. Phys.* **2015**, *17*, 30805−30816.
(49) Thyrhaug, E.; Schröter, M.; Bukartė, E.; Kühn, O.; Cogdell, R.; Hauer, J.; Zigmantas, D. Intraband Dynamics and Exciton Trapping in the LH2 Complex of Rhodopseudomonas Acidophila. *J. Chem. Phys.* **2021**, *154*, 045102.
(50) Escalante, M.; Lenferink, A.; Zhao, Y.; Tas, N.; Huskens, J.; Hunter, C. N.; Subramaniam, V.; Otto, C. Long-Range Energy Propagation in Nanometer Arrays of Light Harvesting Antenna Complexes. *Nano Lett.* **2010**, *10*, 1450−1457.
(51) Strümpfer, J.; Şener, M.; Schulten, K. How Quantum Coherence Assists Photosynthetic Light-Harvesting. *J. Phys. Chem. Lett.* **2012**, *3*, 536−542.
(52) Baghbanzadeh, S.; Kassal, I. Geometry, Supertransfer, and Optimality in the Light Harvesting of Purple Bacteria. *J. Phys. Chem. Lett.* **2016**, *7*, 3804−3811.
(53) Baghbanzadeh, S.; Kassal, I. Distinguishing the Roles of Energy Funnelling and Delocalization in Photosynthetic Light Harvesting. *Phys. Chem. Chem. Phys.* **2016**, *18*, 7459−7467.
(54) Strek, W. Cooperative Energy Transfer. *Phys. Lett. A* **1977**, *62*, 315−316.
(55) Scholes, G. D. Designing Light-Harvesting Antenna Systems Based on Superradiant Molecular Aggregates. *Chem. Phys.* **2002**, *275*, 373−386.
(56) Freiberg, A.; Rätsep, M.; Timpmann, K.; Trinkunas, G. Dual Fluorescence of Single LH2 Antenna Nanorings. *J. Lumin.* **2004**, *108*, 107−110.
(57) Jang, S.; Rivera, E.; Montemayor, D. Molecular Level Design Principle behind Optimal Sizes of Photosynthetic LH2 Complex: Taming Disorder Through Cooperation of Hydrogen Bonding and Quantum Delocalization. *J. Phys. Chem. Lett.* **2015**, *6*, 928−934.
(58) Sajjad, M. T.; Ruseckas, A.; Samuel, I. D. Enhancing Exciton Diffusion Length Provides New Opportunities for Organic Photovoltaics. *Matter* **2020**, *3*, 341−354.
(59) Firdaus, Y.; Le Corre, V. M.; Karuthedath, S.; Liu, W.; Markina, A.; Huang, W.; Chattopadhyay, S.; Nahid, M. M.; Nugraha, M. I.; Lin, Y.; et al. Long-Range Exciton Diffusion in Molecular Non-Fullerene Acceptors. *Nat. Commun.* **2020**, *11*, 5220.
(60) Amarnath, K.; Bennett, D. I. G.; Schneider, A. R.; Fleming, G. R. Multiscale Model of Light Harvesting by Photosystem II in Plants. *Proc. Natl. Acad. Sci. U.S.A.* **2016**, *113*, 1156−1161.
(61) Bennett, D. I. G.; Fleming, G. R.; Amarnath, K. Energy-Dependent Quenching Adjusts the Excitation Diffusion Length to Regulate Photosynthetic Light Harvesting. *Proc. Natl. Acad. Sci. U. S. A.* **2018**, *115*, E9523−E9531.
(62) Varvelo, L.; Lynd, J. K.; Citty, B.; Kühn, O.; Raccah, D. I. G. B. Simplified Main Text Figure Scripts and Data for "Formally Exact Simulations of Mesoscale Exciton Diffusion in a Light Harvesting 2 Antenna Nanoarray". 2023; DOI: 10.5281/zenodo.7674969.
(63) Varvelo, L.; Lynd, J. K.; City, B.; Raccah, D. I. G. B. Formally Exact Simulations of Mesoscale Exciton Diffusion in a Photosynthetic Aggregate: MesoHOPS. 2023; DOI: 10.5281/zenodo.7659219.

https://doi.org/10.1021/acs.jpclett.3c00086
J. Phys. Chem. Lett. 2023, 14, 3077−3083